Final Draft
of the original manuscript:

Anvari, M.; Scheider, I.; Thaulow, C.:
Simulation of dynamic ductile crack growth using strain-rate and triaxiality-dependent cohesive elements
In: Engineering Fracture Mechanics (2006) Elsevier

DOI: 10.1016/j.engfracmech.2006.03.016

Simulation of Dynamic Ductile Crack Growth using Strain-Rate and Triaxiality Dependent Cohesive Elements

M. Anvari[1], I. Scheider[2] and C. Thaulow[1]
[1] Department of Engineering Design and Materials, NTNU, Trondheim, Norway
[2] GKSS Research Center, Geesthacht, Germany

Abstract

Rate-sensitive and triaxiality-dependent cohesive elements are used to simulate crack growth under quasi-static and dynamic loading conditions. The simulations are performed for a middle-cracked tension M(T) specimen made of an aluminum alloy (6XXX-series). To consider the effect of stress triaxiality and strain rate on the cohesive properties, a single plane strain element obeying the constitutive equations of a rate-dependent Gurson type model has been used. The single element is loaded under various stress biaxiality ratios and strain rates and the obtained stress-displacement curves are considered as traction separation law for the cohesive elements. These curves are used for analyzing the aluminum M(T) specimen. The qualitative effects of constraint, strain rate, inertia and stress waves on the energy absorption of the specimen and crack growth are discussed.

Keywords: Cohesive zone modeling, Dynamic loading, Rate dependency, Stress triaxiality, Rate-dependent Gurson type model

1 Introduction

When a structure is subject to dynamic loading, some additional phenomena compared to quasi-static cases have to be considered. The high speed of deformation introduces stress waves into the structure. Inertia effects become significant and can affect the energy absorption of the structure. Strain rate increases the flow stress and influences the strain hardening of metals. And last, but not least, high local temperature increase due to adiabatic heating reduces the flow strength and counteracts the strain rate hardening. Whether it is a stationary crack subject to impact loading, called "impact fracture", or it is a fast motion of the crack tip, named "fast fracture" [1], the mentioned phenomena can affect the fracture toughness significantly and it is important to have an efficient analysis tool for simulating damage and crack growth including these influences.

Analytical and macroscopic approaches used in fracture mechanics have some limitations with respect to the amount of plasticity allowed at the crack tip, constraint and geometry dependency. As Siegmund and Brocks [2] point out, to the present, "local approaches" are the only really successful methods for prediction of crack growth resistance.

In a local approach, in principle, the parameters of the respective model depend only on the material, and not on the geometry. In this kind of approach, one can simulate ductile fracture either by employing a micromechanical model of damage, which represents the micromechanism of void initiation, growth and coalescence, or by using a phenomenological model for material separation and coupling it to the surrounding undamaged elastic-plastic material. In the former approach, a representative volume element (RVE) or "unit cell" is considered to study the respective mechanism. The most widely known model of this kind for ductile damage calculation is the Gurson-Tvergaard-Needleman or GTN model [3]. Zhang et al. [4] proposed a model called "complete Gurson model" as a combination of GTN and Thomason's coalescence criteria [5]. This model has been used for unit cell calculations in the present article.

A phenomenological local approach used for the numerical simulation of crack propagation is known as the cohesive zone model. The idea is based on the pioneering work by Dugdale [6] and Barenblatt [7] who introduced the strip-yield model. Both authors divided the crack into two parts: One corresponds to the physical length of the crack, which is stress free, and the other one is the fracture process zone, where yielding and degradation of the material occur and which is loaded by a finite stress named cohesive stress. Later developments of cohesive models, particularly in combination with finite element method (e.g. [8–11]), considered the cohesive stress as a function of material separation and not depending on the distance from the crack-tip as Barenblatt did. In a finite element representation of cohesive zone models, cohesive elements are introduced as interface between continuum elements and damage occurs only in the interface elements which obey a constitutive equation named traction separation law (TSL) (Fig. 1). Separation in these elements is calculated from the difference of the displacements of the continuum elements adjacent to them. The maximum opening at which the cohesive element completely fails is called critical separation, δ_0, and is one of the fracture parameters. The other fracture parameter is the maximum traction or cohesive strength, S. The area under the TSL is the energy absorbed by the cohesive element and is known as the cohesive energy, Γ_0:

$$\Gamma_0 = \int_0^{\delta_0} T(\delta) d\delta \tag{1}$$

If the shape of a TSL is known or presumed, having two of the aforementioned parameters is enough to define the cohesive law.

By using cohesive zone modeling in a finite element analysis, it is possible to split the total dissipated energy into energy dissipated by plastic deformation in the process zone and the energy of separation. In this way, it is possible to evaluate the damage and deformation processes separately, but coupled. Besides, by entrusting the nucleation, propagation, branching and other aspects of the fracture behavior of materials to a master cohesive law, the amount of phenomenology is considerably reduced compared to theories of distributed damage. Since a characteristic length is included in the TSL (cohesive energy is the work of separation per unit area), the models with cohesive elements are not mesh dependent, which is always an issue for the GTN models [12].

Cohesive elements used in simulating ductile fracture are supposed to represent the mechanism of nucleation, growth and coalescence of microscopic voids that initiate at the inclusions and second phase particles. The idea of the present contribution is to obtain the cohesive properties by studying the mechanical response of a single element obeying a rate-dependent Gurson type constitutive equation. This sort of mechanism-based cohesive model has also been proposed by other authors, e.g. [12–16]. It is well known that the cohesive strength increases with strain rate ([17–19]) and this implies an increase in stress triaxiality [20, 21]. Using a Gurson type model provides a mean for exploring the effect of stress triaxiality on TSL parameters [12]. Rate sensitivity of the cohesive zone is determined by applying different values of loading speed on the rate-sensitive single element and calculating the cohesive parameters from the mechanical response. A similar procedure is performed by applying different stress ratios on the single element to study the effect of stress trixiality on the TSL parameters. The shape of the TSL, cohesive strength and critical displacement are fitted to meet the results of the single element calculations for various strain rates and triaxialities. The parameters are then used for crack growth simulations of an aluminum middle-cracked tension M(T). In the model, the cohesive elements are both triaxiality- and rate-dependent. Triaxiality-dependent cohesive elements have already been introduced to cohesive elements by Siegmund and Brocks [2], whereas the effect of dynamics on cohesive parameters is usually written by a separation rate dependency, see e.g. [18]. Even though the implementation of a strain rate effect is a bit more complicated than a separation rate, it has the advantages that are described in section 2.3.

Since the measures of strain rate and stress triaxiality are not available in the cohesive elements, they are calculated and transferred from the solid elements adjacent to them, which is performed in a similar way as proposed in [2] for only stress triaxiality values. The technique has also been used for strain-dependent cohesive elements by Tvergaard and Hutchinson [22]. The analyses are performed in quasi-static and dynamic cases. The effects of rate dependency, inertia, constraints and waves on mechanical response of the structure are shown by the load-displacement diagrams and the results are discussed. The influence of the pointed out phenomena on plastic energy dissipation and crack growth are illustrated, too. The influence of adiabatic heating has not been considered in the analyses.

The static and transient dynamic analyses are performed in ABAQUS/Standard non-linear finite element code [23]. The rate-dependent complete Gurson model developed and implemented into ABAQUS as a user defined material (UMAT) subroutine [24] is used for the single element calculations. The cohesive element calculations are performed by a user defined element (UEL) subroutine developed by Scheider [25] and expanded by the present authors for rate and triaxiality-dependent cohesive elements to be used in transient dynamic analysis.

2 Calculations

2.1 Material

Smooth round bars made of aluminum alloy 6XXX series were tested by split-Hopkinson tension bar in SIMLab of NTNU [26]. The experimental stress-strain curves at different strain rates are approximated by the following equation [27] as shown in Fig. 2:

$$\bar{\sigma} = \sigma_0 \left(1 + \frac{\bar{\epsilon}}{\epsilon_0}\right)^N \left(\frac{\dot{\bar{\epsilon}}}{\dot{\epsilon}_0}\right)^m \tag{2}$$

where $\bar{\sigma}$, $\bar{\epsilon}$, σ_0 and ϵ_0 stand for true stress, true plastic strain, yield stress, and a reference strain respectively. $\dot{\bar{\epsilon}}$ and $\dot{\epsilon}_0$ are the strain rate and a reference strain rate, respectively. N is known as strain hardening and m as strain rate hardening exponent. In this formulation, the strength of the material increases with the increase of strain rate. The constitutive bahavior is based on von Mises plasticity with pure isotropic hardening. Viscous, i.e. time dependent effects are not considered. The values considered for the material tested are: $\sigma_0 = 217$ MPa, $\epsilon_0 = 0.002$, $\dot{\epsilon}_0 = 150$ 1/s, N=0.0526, m=0.05. Mass density of aluminum, ρ=2700 Kg/m^3 has been considered in all of the dynamic calculations.

2.2 Single element calculations

For ductile metals, the effective behavior of a unit cell containing a void can be captured by using the Gurson model [28] developed by Tvergaard [29] and Tvergaard and Needleman [3]. The latter, known as GTN uses a fixed critical void volume fraction, i.e. the point where coalescence starts, as a material parameter. Koplik and Needleman [30] showed that this assumption works well only for low stress triaxiality cases, and slightly worse for high stress triaxiality cases, which is the case in front of a crack tip. Zhang et al. [4] introduced the Thomason's coalescence criteria [5] into the Gurson model so that it can predict void coalescence. In their approach which they called "complete Gurson model", they also proposed final void volume fraction to be a function of initial void volume fraction. In the strain-rate sensitive version of the model, the flow stress is a function of local strain rate with the same strain rate hardening exponent as that of the bulk material. Details on the rate-dependent Gurson model is found elsewhere (e.g. [31, 32]).

The question that arises is which of the phenomena influencing ductility because of dynamic loading conditions is more important to be considered in modeling a single Gurson type element. Curran et al. [33] considered rate-sensitive material for a hollow sphere of internal radius, a, subjected to internal constant pressure, P_0. The material was considered to be rigid, perfectly plastic with a viscosity coefficient. Their numerical investigation for aluminum showed that the inertia effect becomes important for quite large voids (larger than 10 μm) and for a wide range of radii a, the maximum rate is governed by the viscous regime only. In other words, as far as void size is smaller than a certain value, inertia can be ignored in modeling void growth under dynamic loading. Considering the work done by Johnson [34], it is concluded that the inertia effect is important in void growth only if the

speed of crack growth is higher than $4\sqrt{\sigma_0/\rho}$ where σ_0 and ρ are the flow stress and the density of the material, respectively. This value is around 1100 m/s for a typical aluminum alloy. Liu [35] also showed that increasing strain rate will increase the inertia effect, but this effect is significant only when the strain rate is over 10000 1/s.

Based on these discussions, only rate sensitivity of the material has been considered. The effect of the adiabatic heating is ignored in all of the calculations.

In the present study, a single four node plane strain element with rate-dependent complete Gurson model as constitutive equation is used. The initial void volume fraction of $f_0 = 0.002$ is considered in the calculations as suggested in [36], since no experimental data on micromechanical information is available for this parameter. The analyses are performed for an element with the initial size of h×h, h=1 mm, for different stress biaxialities β, as shown in Fig. 3:

$$\beta = \frac{\sigma_{11}}{\sigma_{22}} \tag{3}$$

If the material is incompressible, the stress triaxiality which is the ratio between mean normal stress and von-Mises equivalent stress is given by [12]:

$$H \approx \frac{1+\beta}{\sqrt{3}\,(1-\beta)} \tag{4}$$

The constant stress ratios in static loadings were obtained using modified Riks method implemented in ABAQUS. The reason for using Riks method is the instability in load controlled calculations due to softening. Figure 3 shows the normalized traction separation obtained for different values of triaxiality. Figure 4 shows the variation of normalized strength and energy obtained from Fig. 3 versus triaxiality. The curves are fitted to the calculated values.

In order to investigate the effect of strain rate on the stress-elongation behavior, quasi-static analyses were performed with a rate-dependent model and high speed loading. Since strain rate was considered, Riks method was not applicable any more. Thus, two linear springs were added to the model and the multi-point constraint (MPC) subroutine in ABAQUS was used to obtain constant stress ratios. For low speed of applied loads, the responses were the same as the Riks method. Figure 5 shows the normalized traction-separation behavior for different triaxialities for a loading rate of 500 mm/s or, in other words, an initial strain rate of 500 1/s for an element of initial length h=1 mm. The figure shows that the effect of triaxiality is similar to the case with rate-independent material behavior, but the values of cohesive strength and consequently cohesive energy are different. To check this, various loading speeds were applied for the same triaxiality of 1.5 (β=0.44). Figure 6 shows that the curves are parallel and only the value of strength changes for the same maximum displacement. Figure 7 shows the curves fitted to the calculated values of strength and energy for the rate-dependent case at constant loading rate (V=500 mm/s) and different triaxiality values. Comparing this figure with Fig. 4, it is observed that the fitted curves are very similar to the rate insensitive case.

Figure 8 shows how the values of cohesive strength and cohesive energy change with loading rate for a constant triaxiality of 1.5. As it is shown, the value of the maximum trac-

tion changes as a function of the rate independent case for the same triaxiality multiplied by the relative strain rate to the power of m (strain rate hardening exponent).

2.3 Traction separation law

Since the cohesive model is a phenomenological model, authors use various formulations for defining the shape of TSL and the cohesive values (e.g. [8,10,13,37–39]). Among these definitions, the one introduced by Scheider and Brocks [39] has been used to reproduce the calculated damage and failure of the unit cell by a cohesive element. This TSL has two shape parameters, δ_1 and δ_2, in addition to the cohesive parameters already introduced and consists of three parts: (a) increasing traction or cohesion, (b) constant traction and (c) decreasing traction or decohesion (see Figure 9). The traction as a function of the separation in this model is:

$$T = S \begin{cases} 2\left(\frac{\delta}{\delta_1}\right) - \left(\frac{\delta}{\delta_1}\right)^2 & ,0 < \delta < \delta_1 \\ 1 & ,\delta_1 < \delta < \delta_2 \\ 2\left(\frac{\delta-\delta_2}{\delta_0-\delta_2}\right)^3 - 3\left(\frac{\delta-\delta_2}{\delta_0-\delta_2}\right)^2 + 1 & ,\delta_2 < \delta < \delta_0 \end{cases} \tag{5}$$

By changing δ_1 and δ_2, one can have a variety of TSL shapes. In this formulation, the maximum separation is:

$$\delta_0 = \frac{2\Gamma_0}{S} \frac{1}{1 - \frac{2}{3}\frac{\delta_1}{\delta_0} + \frac{\delta_2}{\delta_0}} \tag{6}$$

Although it has been claimed that the shape of the TSL hardly influences the crack growth behavior [13,37,40,41], there are a few investigations that show higher effects of the shape [19,42,43]. For example, Scheider and Brocks [42] showed numerically that not only the shape of the TSL can affect the load-displacement behavior, but also the TSL shapes that make the same results in a fracture specimen, might make different results in another specimen. Falk et al. [43] showed that if the TSL is initially rigid, the model can not capture crack branching by using a regular finite element mesh and it is possible when the TSL has initial elasticity.

Regarding uncertainties like these, rate-dependent Gurson type model has been used as the basis for obtaining the TSL.

It is possible to obtain the following expressions for the cohesive strength and energy using the mathematical approximations shown in Figs. 4, 7 and 8 as:

$$\frac{\Gamma_0}{h} \approx 1.43 H^{-1.36} \sigma_0 \left(\frac{\dot{\bar{\epsilon}}}{\dot{\epsilon}_0}\right)^m \tag{7}$$

$$S \approx (1.1\, ln(H) + 2.1)\, \sigma_0 \left(\frac{\dot{\bar{\epsilon}}}{\dot{\epsilon}_0}\right)^m \tag{8}$$

The variable h is the characteristic length scale of the Gurson model, which is usually based on the micromechanical structure of the material. A value of h=0.1 mm is chosen

in accordance to [44] who also investigated an aluminum alloy of 6XXX series. H is the stress triaxiality. The expression in Eq. (8) is similar to the results obtained analytically by Zhang et al. [19] which show that the curves of normalized traction along the cohesive zone are parallel at various crack speeds and the cohesive strength increases with crack growth rates. It has also been pointed out by Freund [45] that as the crack moves more rapidly, the material is deformed more rapidly and a larger cohesive stress is required in order to achieve the requisite crack tip opening displacement.

Considering e.g. Fig. 5, it is recognizable that the piecewise TSL defined by Eq. (5) and shown in Fig. 5 fits properly to the curves if the shape parameters δ_1 and δ_2 are adjusted accordingly. Combining Eqs. (6), (7) and (8), the critical separation reads:

$$\frac{\delta_0}{h} \approx \frac{2.8H^{-1.36}}{1.1\,ln(H)+2.1}\,\frac{1}{1-\frac{2}{3}\frac{\delta_1}{\delta_0}+\frac{\delta_2}{\delta_0}} \tag{9}$$

The comparison between the stress elongation behavior obtained from rate-dependent Gurson model calculations and the TSL approximation of Eq. (5) with the cohesive parameters from Eqs. (8) and (9) and $\frac{\delta_1}{\delta_0}$=0.07 and $\frac{\delta_2}{\delta_0}$=0.35 are shown in Fig. 10 for two different triaxiality values. Since the curves obtained from the single element calculations and those based on Eq. (9) are not exactly the same, the critical displacements are a slightly different for the same cohesive strength and energy, but the differences are reasonable.

It is worth noting that the initial stiffness of the cohesive elements is relatively high. Therefore, the separations are very small in the beginning until the cohesive strength is reached. This is an important indication for the use of a strain rate instead of a separation rate dependent cohesive model. The cohesive strength is strongly influenced by the rate, and in the beginning most of the deformation takes place in the adjacent continuum elements whereas the cohesive elements are still closed. On the other hand, the effect of the rate on the softening branch of the traction separation law is of minor importance since the characteristic of the damage behavior is then more affected by the cohesive energy parameter which is not much dependent on strain rate, see Figs. 6 and 8.

3 Crack growth simulations and results

An M(T) specimen of unit thickness and dimensions of 100×100 mm^2 has been modeled using four node plane strain elements. The ratio of the initial crack length to the specimen's width is $a/W = 0.5$. One row of cohesive elements with initial zero height has been used at the ligament. Because of symmetry, one fourth of the specimen has been modeled. Figure 11 shows the specimen and the detailed mesh at the crack tip and a part of the ligament. The smallest continuum element size belongs to the elements adjacent to the ligament and it is 0.1×0.1 mm^2.

The surrounding continuum elements behave according to Eq. (2) and the cohesive elements based on Eqs. (5), (7), (8) and (9). Each cohesive element possesses four nodes and two integration points. Because of the symmetry, only the two upper nodes of cohesive elements are shared with the adjacent continuum element and the other two obey the

displacement conditions of symmetry. For each cohesive element, the actual values of nodal displacement, triaxiality and strain rate are used to compute the current value of traction and element stiffness. The values of triaxiality and strain rate are calculated in the continuum elements along the ligament at all of the integration points using UVARM subroutine in ABAQUS. The averages of these values are then calculated after the load increment and provided to the respective adjacent cohesive elements in the next increment as shown in Fig. 12. The error of this kind of explicit scheme is accepted since the time increments are always chosen to be small enough.

Material separation process involving void growth and plastic deformation at microlevel are irreversible by nature. This property has been implemented in the cohesive element formulation in a sense that a separation already happened to an element remains after local unloading and relaxing the stress [25]. Local unloading can happen because of global unloading, stress waves or crack branching.

The simulations performed are described in Table 1. The aim of the analyses is to check the influence of constraint, rate sensitivity, inertia and elastic waves on the energy absorption of a typical M(T) specimen. In the static simulations, the effect of triaxiality on the energy absorption is studied. In the dynamic analyses, denoted by DYN-xxx, the effects of inertia and elastic waves are investigated as well as the influence of stress triaxiality and rate sensitivity.

Figure 4 shows that the change of cohesive energy (critical displacement) is very high for triaxiality values of H <1.5. The reason is that for small values of triaxiality, the initial void grows very little and therefore the energy absorbed is mostly related to the plastic deformation and not damage in the cell model. For more detailed discussions on the limitations of the application of cell model and the competition between cohesive process zone and plastic flow, see [20]. It is also known that the M(T) specimen is a low constraint fracture specimen. The analyses show that the stress triaxiality at the crack tip increases while the crack is growing. Regarding these discussions, $H = 1.2$ was considered as an initial stress triaxiality value used in the simulations. Below this value, the cohesive parameters were considered to be constant, i.e.:

$$\frac{\Gamma_0}{h} = \begin{cases} 237.6 \left(\frac{\dot{\epsilon}}{\dot{\epsilon}_0}\right)^m & , H < 1.2 \\ Eq.\ 7 & , H \geq 1.2 \end{cases} \tag{10}$$

$$S = \begin{cases} 474 \left(\frac{\dot{\epsilon}}{\dot{\epsilon}_0}\right)^m & , H < 1.2 \\ Eq.\ 8 & , H \geq 1.2 \end{cases} \tag{11}$$

The cohesive parameters for $H = 1.2$ were also used for the triaxiality independent analyses.

The load was applied as a prescribed displacement at the upper edge of the specimen. In dynamic cases, the speed of the load was 3.3 m/s. The load and displacements presented in the following diagrams are the values calculated on the boundary of the model.

Figure 13 shows load-displacement curves for quasi-static solutions. The figure shows that ignoring triaxiality dependency of interface elements can lead a static crack growth analysis to be highly conservative, because the prediction of the energy absorption is much

lower than the constraint (stress triaxiality) dependent case. This shows that the values of triaxiality increase to more than the initial value considered in the analyses.

Figure 14 shows the load-displacement curves obtained from dynamic analyses. Since transient dynamic solution has been employed, inertia and elastic waves are inherent in the analyses. The existence of oscillations in the curves is inevitable because of the existence of elastic waves. The time that elastic waves travel the length of the specimen is around 20 μs; that is much shorter than the total time of fracture (the shortest time of fracture is 131.8 μs, which is for the case of rate dependent bulk material). The elastic waves can have two sources, one is the dynamically applied load and the other is the wave induced by broken cohesive elements or, in other words, the waves induced because of the relatively high speed of the crack growth. Because of the implicit integration used in the dynamic analyses, there is no severe limitation on the time increment chosen. Repeating one of the simulations with very short maximum allowable time increments (0.02 μs instead of 24 μs) showed that the averaged results are similar, but the rate of convergence is very low and the simulation is extremely time consuming.

Dynamic simulation considering the rate dependency only for bulk material leads to the most conservative assumption. Ignoring the effect of strain rate and triaxiality on the behavior of interface elements makes the results unrealistic. Using rate- and triaxiality-dependent cohesive elements results in more energy absorption, although it is less than the simulation which ignores all of these influences.

Figure 15 shows the crack growth vs. time for dynamic simulations. In all of the cases, the crack speed is low in the beginning and then it increases to a somewhat steady state speed. The case with no rate dependency is an exception in it seems that the crack speed is changing during the growth. The figure shows clearly that the steady state speed of the crack growth is highest, about 1430 m/s, for the case in which only bulk material is rate dependent. If an average speed is defined for the case with no rate dependency, the lowest crack growth speed of around 290 m/s is obtained for this case. It should be noted that for the case where both bulk material and cohesive zone are rate dependent, the crack growth initiation happens almost at the same time as for the case with no rate dependency. This is in contrast to the investigations of Basu [46] who numerically showed that strain rate sensitivity plays a beneficial role on dynamic ductile fracture initiation. This contradiction is related to ignoring triaxiality change even at the first stages of deformation. It is observed in Fig. 15 that when triaxiality dependency is considered, crack growth initiation happens at 69 μs which is higher than the rate-insensitive case. To check if this effect is due to the rate sensitivity of the material, a dynamic case was simulated with triaxiality-dependent cohesive elements while no rate sensitivity was considered. The analysis showed that the crack growth initiation happened at 61.8 μs. This proves that rate sensitivity has postponed crack growth initiation, although after a short time, crack growth speed is higher than the rate-insensitive case. It should also be noted that in the case where stress triaxiality change has been ignored, the crack growth velocity becomes so high that the assumption of ductile mechanism of crack growth might be inaccurate. It is worth noting that for the case in which only rate dependency of bulk material has been considered, the crack speed is around 1400 m/s. In this case, the inertia effect on fracture energy is

important, but it has been ignored in the calculation. Regarding these discussions and back to Fig. 14, it is well understood why the load in the triaxiality and rate dependent case is higher in the beginning and drops very fast after some time. This is qualitatively compatible with Freund's finding [45]. He used a rate sensitive cohesive zone and showed analytically, with some assumptions on the amount of plasticity and material behavior, that for high speed of crack growth (more than about 20% of shear wave propagation velocity), "as the crack tip speed increases for some fixed level of viscosity (rate sensitivity), the local stress is elevated and a smaller applied stress intensity factor is required for crack growth". He also showed that for lower crack speeds or smaller viscosities, however, the criteria is reversed.

The reason why crack speed is much higher in the case of rate-dependent plasticity is that the material hardens due to high loading rate and opens the crack (cohesive elements) more easily. Figure 16 shows the ratio of dissipated plastic energy to the external work vs. crack growth. This figure shows that for the rate sensitive material, the percentage of the energy absorbed by the plastic deformation is less compared to the rate insensitive case and the difference increases with crack growth. When the cohesive zone is rate dependent, the cohesive strength is increased at high loading rates and this causes more energy dissipated by plasticity in the surrounding material. Although the stresses needed for crack propagation are higher compared to the case with rate independent cohesive parameters, the cohesive strength, S, is not high enough to decrease the crack growth rate as much as for the rate insensitive case. The reason is that with increasing plasticity, the crack opening speed decreases, so the local strain rate and consequently the cohesive strength decrease again. Besides, stress triaxiality increases initially, but because of inertia it decreases while the crack is growing [47]. This means that the decrease of the cohesive strength is related to the inertia. Figure 17 shows the change of triaxiality value during crack growth for the case in which rate dependency and triaxiality have been considered for the cohesive elements.

Figure 18 shows how the phenomena mentioned in the introduction part affect the mechanical response of the structure and makes it clear that the effect of the combination of them is not easily predicted. It demonstrates that although rate dependency and inertia can increase the maximum load in a displacement-controlled loading, rate dependency decreases the total energy absorption of the specimen. This is in contrast to an uncracked specimen in which rate dependent plasticity and inertia increase the energy absorption under dynamic loading.

It was already mentioned that models with cohesive elements are mesh independent, but since an average of field variables is calculated in the adjacent continuum element, this average may depend on the element size. To check the influence of rate-sensitive cohesive elements on the mesh dependency of the model, the specimen was also modeled by element size of 0.05×0.05 mm^2 for the continuum elements adjacent to the ligament. Figure 19(a) shows the load-displacement curves for the two models. It is observed that the effect is insignificant and only exists in the last part of the deformation. Figure 19(b) shows that the crack growth rates are similar up to some time and then the crack growth speed is slightly higher in the model with finer mesh. With the element sizes considered in the present

models, mesh density is not very important, especially for the global energy absorption predicted. It should be noted that although cohesive zone models are theoretically mesh independent, the mesh must not be so coarse that the calculation of local plastic strain field is imprecise or mesh dependent [48].

4 Conclusion

The effect of triaxiality and strain rate on cohesive properties has been considered simultaneously in a finite element dynamic crack growth simulation. Cohesive strength increases with strain rate and this implies an increase in stress triaxiality. Taking into account the interaction between these influences to solve dynamic crack growth problems in a closed form is not an easy task to do. The change of cohesive properties with these variables has been obtained through calculations on a cell model obeying rate-dependent Gurson constitutive equation. The results of the calculations have been used in crack growth simulations of a center-cracked specimen under static and dynamic loading. The procedure has the ability to take into account the effect of stress triaxiality, strain rate and inertia in a proper and relatively simple way. The general results are:

(1) In a quasi-static loading, triaxiality increases with crack growth, but in dynamic cases it increases initially whereas inertia leads to its decrease during crack growth.

(2) Although strain rate sensitivity makes a ductile crack initiation to be postponed, it leads to a faster crack growth due to a decrease in the amount of plasticity at the crack tip area. In other words, although the energy absorption increases initially, it drops very fast after a short crack growth. This is in contrast with a dynamically loaded uncracked specimen, where positive strain rate sensitivity always makes the specimen absorb more energy.

(3) In the dynamic analyses performed, the presumption of ductile fracture will be inaccurate if the change of triaxiality is ignored.

(4) Considering strain rate in the dynamic simulations while ignoring the stress triaxiality leads to a high underestimation of the toughness.

(5) The global energy absorption of the specimen with rate sensitive cohesive elements is not highly mesh dependent. This is valid as long as the mesh is fine enough to calculate plastic stress distribution correctly.

These results are compatible with other studies in this field which have used different approaches.

Acknowledgment

The authors from NTNU would like to acknowledge Hydro Aluminium and the Research Council of Norway for their support through the NorLight project. The first author appreciates the scientific and friendly atmosphere in WMS department at GKSS research center during his stay. He also gives his special thanks to professor Wolfgang Brocks for

his precious support and advises.

References

[1] T. Nishioka. Computational dynamic fracture mechanics. *International Journal of Fracture*, 86:127–159, 1997.

[2] T. Siegmund and W. Brocks. A numerical study on the correlation between the work of separation and the dissipation rate in ductile fracture. *Engineering Fracture Mechanics*, 67:139–154, 2000.

[3] V. Tvergaard and A. Needleman. Analysis of the cup-cone fracture in a round tensile bar. *Acta Metallurgica*, 32:157–169, 1984.

[4] Z.L. Zhang, C. Thaulow, and J. Ødegård. A complete Gurson model approach for ductile fracture. *Engineering Fracture Mechanics*, 67:155–168, 2000.

[5] P.F. Thomason. *Ductile fracture of metals.* Pergamon Press, Oxford, 1990.

[6] D.S. Dugdale. Yielding of steel sheets containing slits. *Journal of the Mechanics and Physics of Solids*, 8:100–104, 1960.

[7] G.I. Barenblatt. The mathematical theory of equilibrium cracks in brittle fracture. *Advances in Applied Mechanics*, 7:55–129, 1962.

[8] A. Hillerborg, M. Modéer, and P.E. Petersson. Analysis of crack formation and crack growth in concrete by means of fracture mechanics and finite elements. *Cement and Concrete Research*, 6:773–782, 1976.

[9] P.E. Petersson. Crack growth and development of fracture zones in plain concrete and similar matrials. Technical report, Report LUTVDG/TVBM-1006, Lund Institute of Technology, 1981.

[10] A. Needleman. A continuum model for void nucleation by inclusion debonding. *Journal of Applied Mechanics*, 54:525–531, 1987.

[11] V. Tvergaard. Material failure by void growth to coalescence. *Advances in Applied Mechanics*, 27:83–151, 1990.

[12] T. Siegmund and W. Brocks. Predictions of the work of separation and implications to modeling. *International Journal of Fracture*, 99:97–116, 1999.

[13] V. Tvergaard and J.W. Hutchinson. The relation between crack growth resistance and fracture process parameters in elastic-plastic solids. *Journal of the Mechanics and Physics of Solids*, 40:1377–1397, 1992.

[14] W. Brocks, D.Z. Sun, and A. Hönig. Verification of the transferability of micromechanical parameters by cell model calculations for visco-plastic materials. *International Journal of Plasticity*, 11:971–989, 1995.

[15] K.B. Broberg. The cell model of materials. *Computational Mechanics*, 19:447–452, 1997.

[16] V. Tvergaard. Crack growth predictions by cohesive zone model for ductile fracture. *Journal of the Mechanics and Physics of Solids*, 49:2191–2207, 2001.

[17] F. Costanzo and J.R. Walton. Numerical simulations of a dynamically propagating crack with a nonlinear cohesive zone. *International Journal of Fracture*, 91:373–389, 1998.

[18] A. Corigliano and M. Ricci. Rate-dependent interface models: formulation and numerical applications. *International Journal of Solids and Structures*, 38:547–576, 2001.

[19] X. Zhang, Y.W. Mai, and R.G. Jeffrey. A cohesive plastic and damage zone model for dynamic crack growth in rate-dependent materials. *International Journal of Solids and Structures*, 40:5819–5837, 2003.

[20] K.B. Broberg. Influence of T-stress, cohesive strength and yield strength on the competition between decohesion and plastic flow in a crack edge vicinity. *International Journal of Fracture*, 100:133–142, 1999.

[21] M.P. Wnuk and J. Legat. Work of fracture and cohesive stress distribution resulting from triaxiality dependent cohesive zone model. *International Journal of Fracture*, 114:29–46, 2002.

[22] V. Tvergaard and J.W. Hutchinson. Effect of strain-dependent cohesive zone model on predictions of crack growth resistance. *International Journal of Solids and Structures*, 33(20-22):3297–3308, 1996.

[23] ABAQUS. *ABAQUS Version 6.4*. H.K.S. Inc. Pawtucket, U.S.A., 2003.

[24] Z.L. Zhang. *A practical micro-mechanical model-based local approach methodology for the analysis of ductile fracture of welded T-joints*. Lappeenranta University of Technology, Finland, Ph.D. Thesis, 1994.

[25] I. Scheider. Cohesive model for crack propagation analyses of structures with elastic-plastic material behavior. Foundations and implementation. Technical report, GKSS internal report no. WMS/2000/19, 2000.

[26] A.H. Clausen and T. Auested. Split-Hopkinson tension bar, experimental set-up and theoretical considerations. Technical report, SIMLab internal report no. R-16-02, 2002.

[27] J. Pan, M. Saje, and A. Needleman. Localization of deformation in rate sensitive porous plastic solids. *International Journal of Fracture*, 21:261–278, 1983.

[28] J. Gurson. Continuum theory of ductile rupture by void nucleation and growth. Part I-yield criteria and flow rules for porous ductile media. *Journal of Engineering and Materials Technology*, 99:2–15, 1977.

[29] V. Tvergaard. On localization in ductile materials containing spherical voids. *International Journal of Fracture*, 18:237–252, 1982.

[30] J. Koplik and A. Needleman. Void growth and coalescence in porous plastic solids. *International Journal of Solids and Structures*, 24:835–853, 1988.

[31] A. Needleman and V. Tvergaard. An analysis of dynamic, ductile crack growth in a double edge cracked specimen. *International Journal of Fracture*, 49:41–67, 1991.

[32] D. Z Sun, A. Hönig, W. Böhme, and W. Schmitt. Application of micromechanical models to the analysis of ductile fracture under dynamic loading. In F. Erdogan and R.J. Hartranft, editors, *Fracture Mechanics: 25th Syp., ASTM STP 1220*, pages 343–357, American Society for Testing and Materials, Philadelphia, 1994.

[33] D.R. Curran, L. Seaman, and D.A. Shockey. Dynamic failure of solids. *Physics Reports*, 147:253–388, 1987.

[34] J.W. Johnson. Dynamic fracture and spallation in ductile solids. *Journal of Applied Physics*, 52(4):2812–2825, 1981.

[35] J. Liu. *A new dynamic void growth model*. Norwegian University of Science and Technology, Norway, Doctoral Thesis, 2004.

[36] G. Bernauer and W. Brocks. Micro-mechanical modelling of ductile damage and tearing - results of a european numerical round robin. *Fatigue and Fracture of Engineering Materials and Structures*, 25:463–384, 2002.

[37] A. Needleman. An analysis of decohesion along an imperfect interface. *International Journal of Fracture*, 42:21–40, 1990.

[38] G.V. Guinea, J. Planas, and M. Elices. A general bilinear fit for the softening curve of the concrete. *Materials and Structures*, 27:99–105, 1994.

[39] I. Scheider and W. Brocks. Simulation of cup-cone fracture using the cohesive model. *Engineering Fracture Mechanics*, 70:1943–1961, 2003.

[40] T. Siegmund and A. Needleman. A numerical study of dynamic crack growth in elastic-viscoplastic solids. *International Journal of Solids and Structures*, 34:769–787, 1997.

[41] G. Lin, A. Cornec, and K.H. Schwalbe. Three-dimensional finite element simulation of crack extension in aluminum alloy 2024-FC. *Fatigue and Fracture of Engineering Materials and Structures*, 21:1159–1173, 1998.

[42] I. Scheider and W. Brocks. The effect of the traction separation law on the results of cohesive zone crack propagation analyses. *Key Engineering Materials*, 251-252:313–318, 2003.

[43] M. Falk, A. Needleman, and J.R. Rice. A critical evaluation of cohesive zone models of dynamic fracture. *Journal de Physique IV France*, 11:43–50, 2001.

[44] P. Négre, D. Steglich, and W. Brocks. Crack extension in aluminium welds: a numerical approach using the gurson-tvergaard-needleman model. *Engineering Fracture Mechanics*, 71(71):2365–2383, 2004.

[45] L.B. Freund. *Dynamic fracture mechanics*. Cambridge University Press, 1998.

[46] S. Basu and R. Narashimhan. Finite element simulation of mode I dynamic, ductile fracture initiation. *International Journal of Solids and Structures*, 33(8):1191–1207, 1996.

[47] S. Basu and R. Narashimhan. A numerical investigation of loss of crack tip constraint in a dynamically loaded ductile specimen. *Journal of the Mechanics and Physics of Solids*, 48:1967–1985, 2000.

[48] A. Needleman. Numerical modeling of crack growth under dynamic loading conditions. *Computational Mechanics*, 19:463–469, 1997.

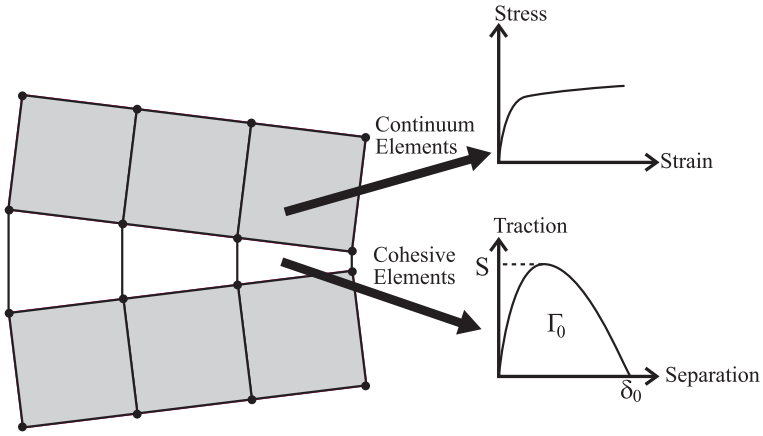

Figure 1: Cohesive zone obeying a TSL and the surrounding undamaged elastic-plastic material

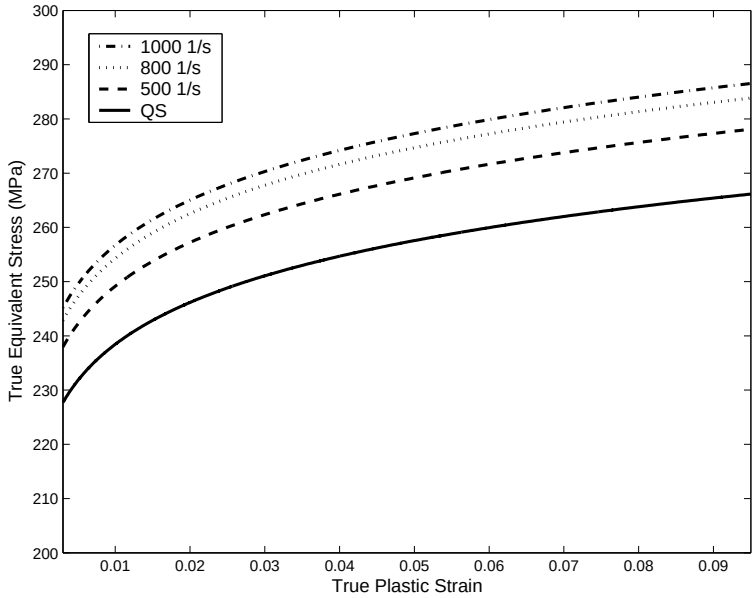

Figure 2: The experimental stress strain curves for different strain rates approximated by Eq. (6)

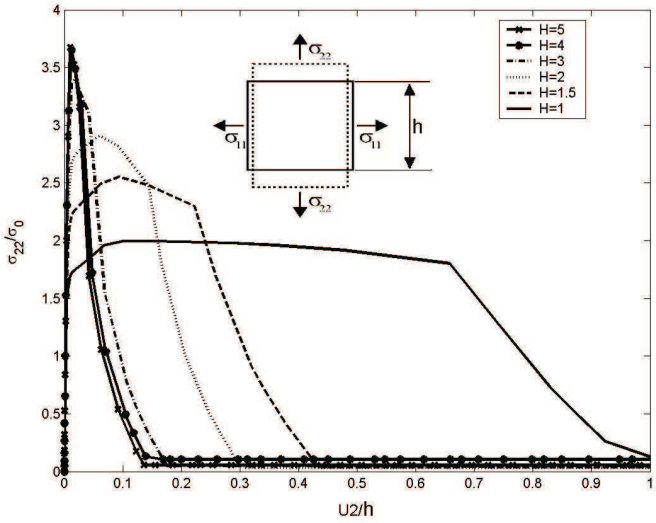

Figure 3: The effect of triaxiality on the traction separation behavior of a single element obeying complete Gurson model

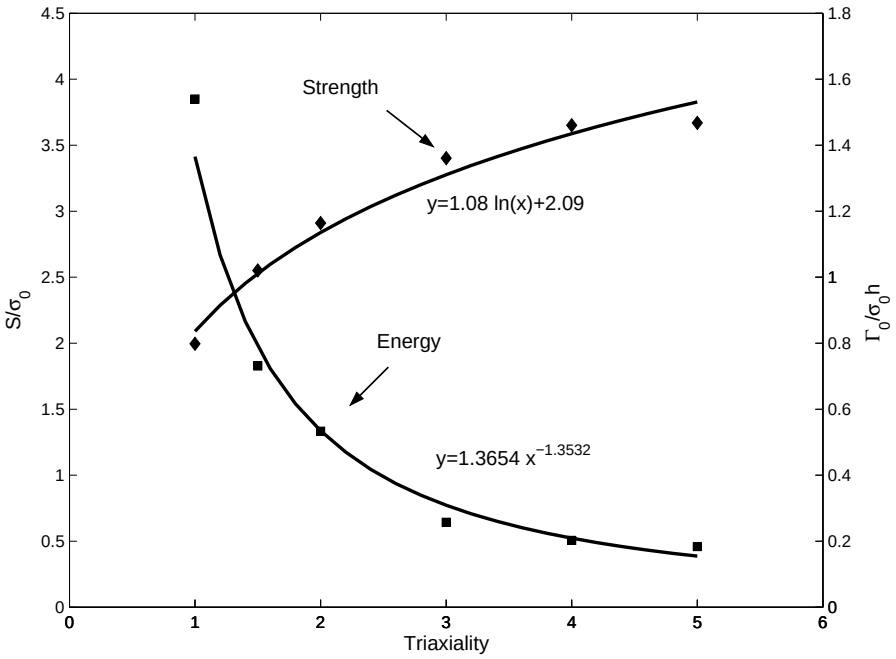

Figure 4: Variation of normalized cohesive strength and cohesive energy versus applied triaxiality for rate insensitive material

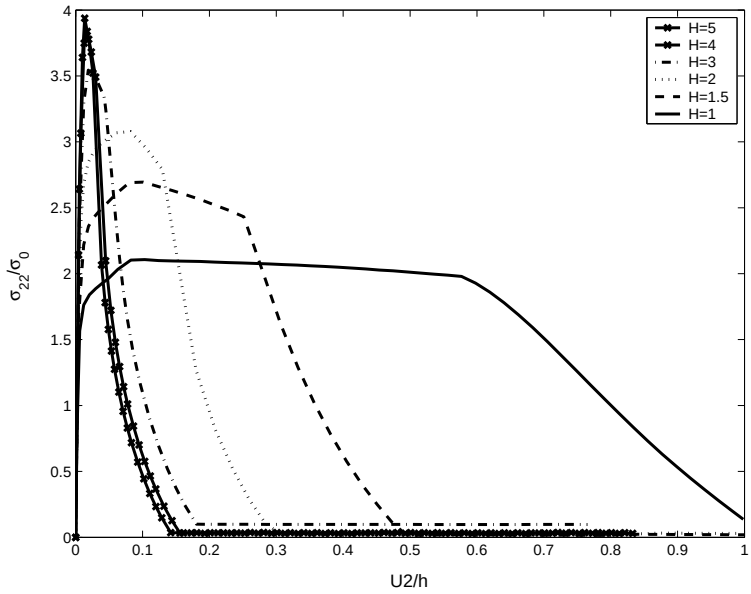

Figure 5: Normalized traction separation behavior in different triaxialities for a load speed of 500 mm/s (initial strain rate of 500 1/s)

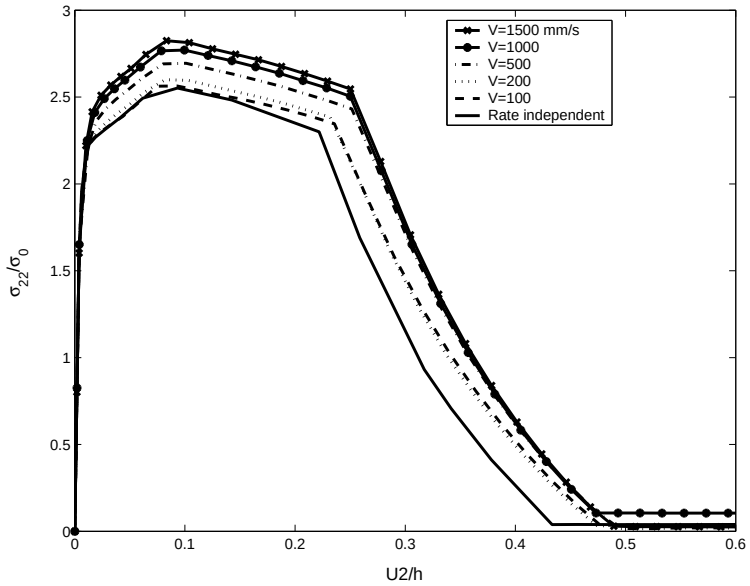

Figure 6: Normalized traction separation behavior at different load speeds (initial strain rate) and constant triaxiality (H=1.5)

Table 1: Various simulations of M(T) specimen

Case	**Analysis**	**Plasticity**	**Cohesive Zone**
QS	Quasi-static	Rate independent	Constant
$QS-CTD$	Quasi-static	Rate independent	Triaxiality dependent
DYN	Transient dynamic	Rate independent	Constant
$DYN-MRD$	Transient dynamic	Rate dependent	Constant
$DYN-MCRD$	Transient dynamic	Rate dependent	Rate dependent
$DYN-MCRD-CTD$	Transient dynamic	Rate dependent	Rate AND triaxiality dependent

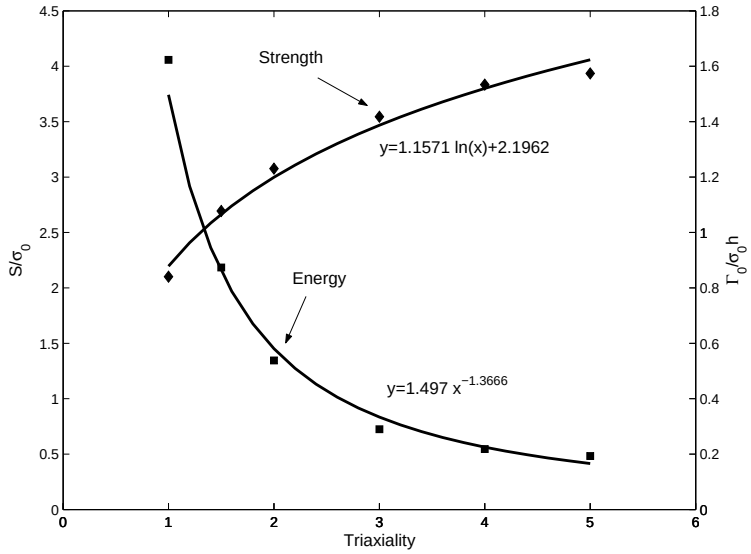

Figure 7: Variation of normalized cohesive strength and normalized cohesive energy versus different triaxialities in constant load speed of 500 mm/s

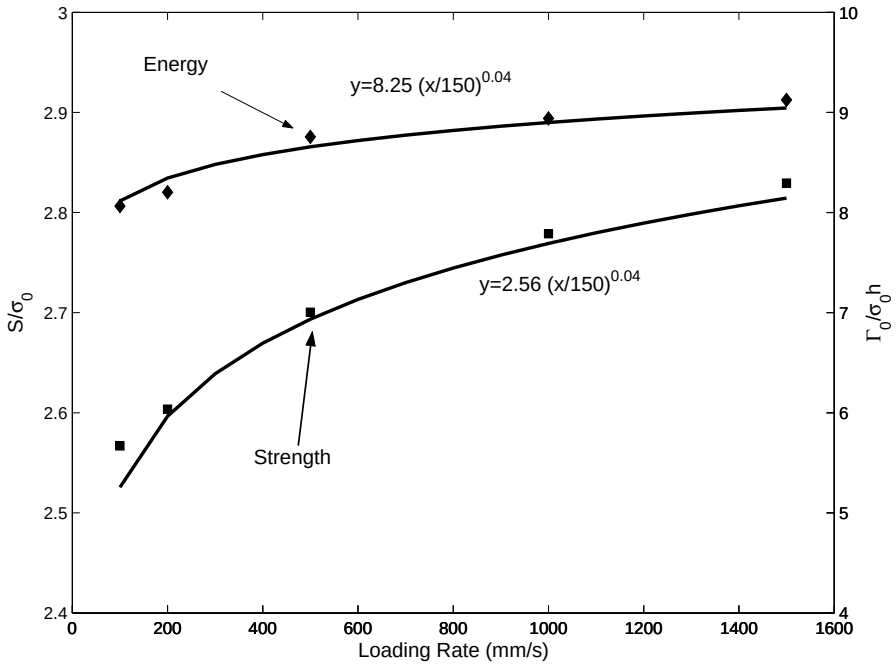

Figure 8: Cohesive strength and cohesive energy versus load speed for a constant triaxiality of 1.5

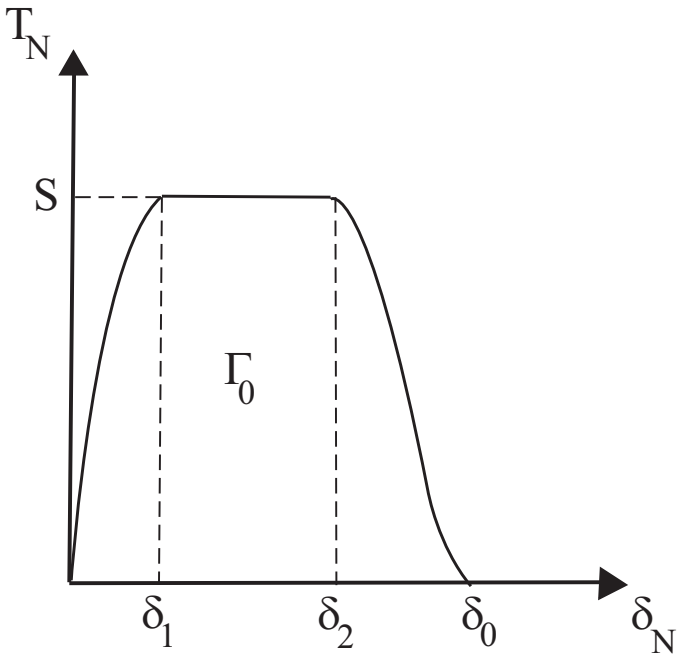

Figure 9: TSL shape proposed by Scheider and Brocks (2003).

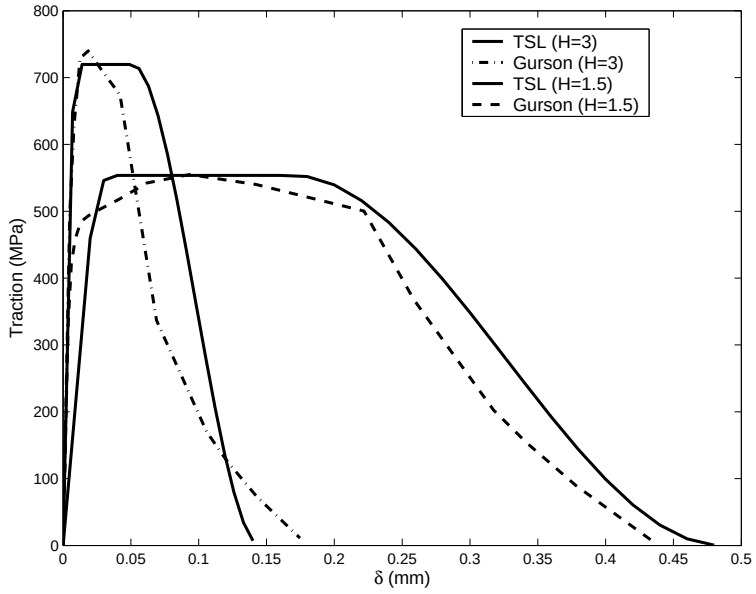

Figure 10: A comparison between traction separation behavior obtained from Gurson type model and the TSL proposed in Eq. (5)

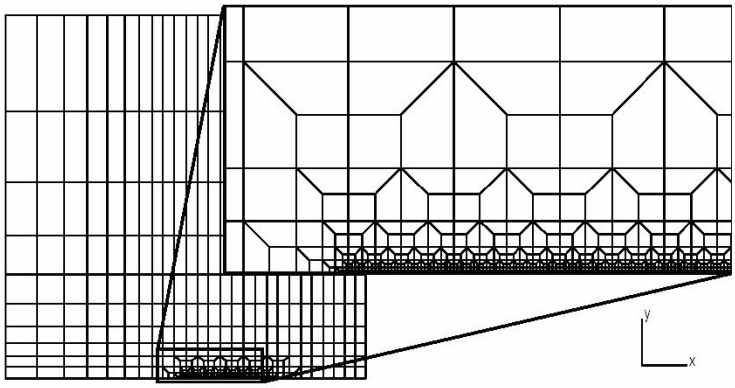

Figure 11: The M(T) specimen and a detailed finite element model of the crack tip

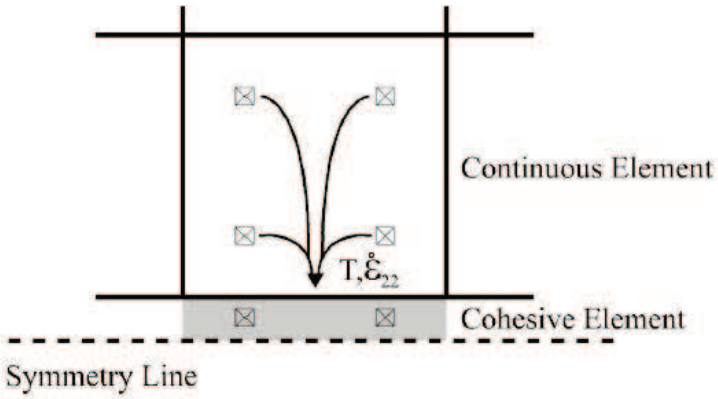

Figure 12: The triaxiality and strain rate values are transferred to cohesive elements from the adjacent continuum elements

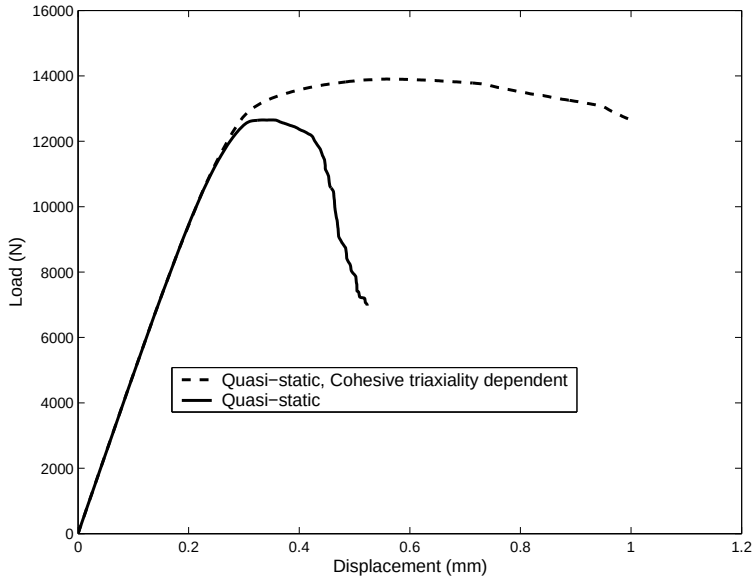

Figure 13: The effect of constraint on the load-displacement behavior (static analysis)

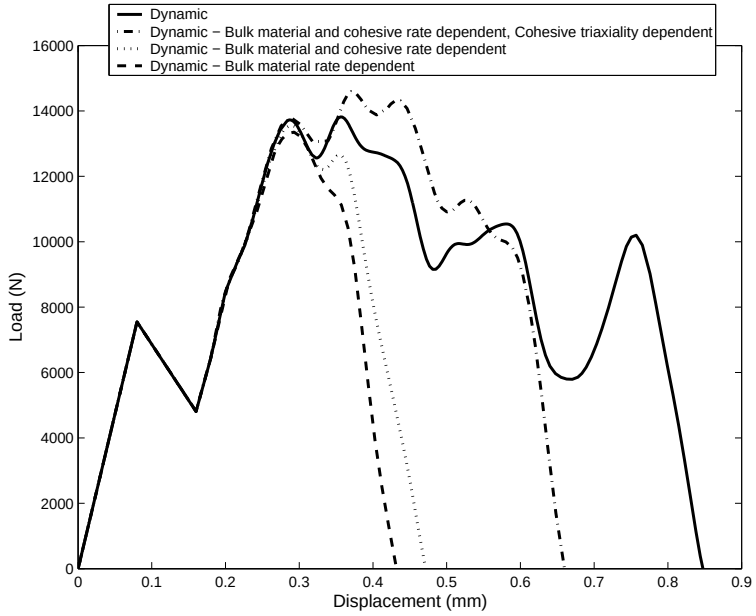

Figure 14: The effect of strain rate and constraint on the load-displacement behavior (dynamic analysis)

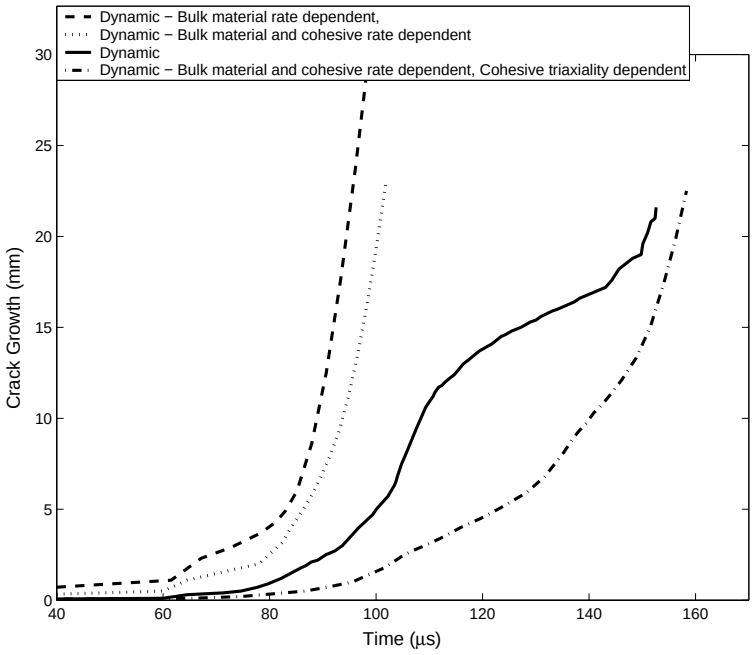

Figure 15: The effect of strain rate and constraint on crack growth rate (dynamic loading)

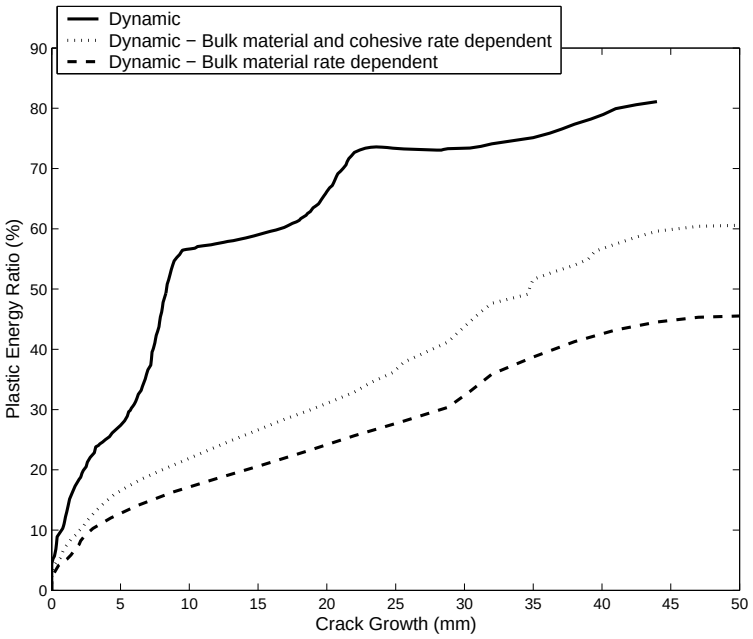

Figure 16: The effect of strain rate sensitivity on percentage of energy dissipated by plastic deformation during crack growth

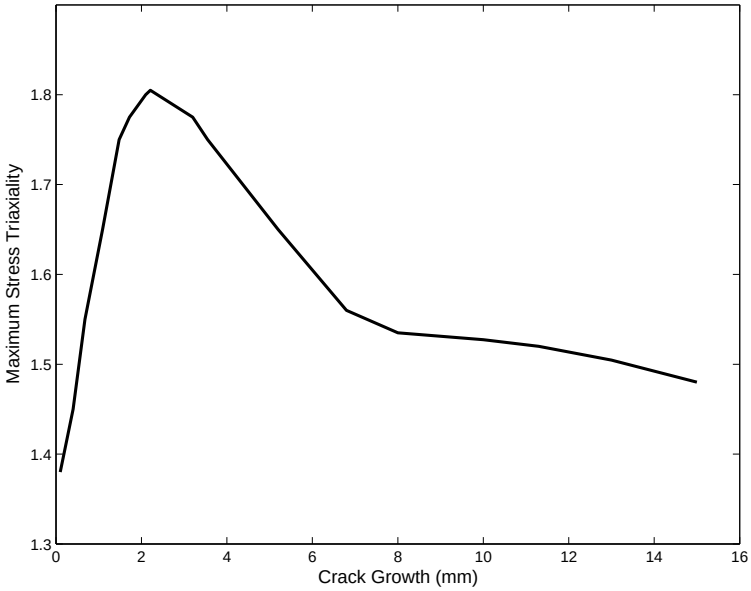

Figure 17: The change of stress triaxiality during crack growth under dynamic loading conditions

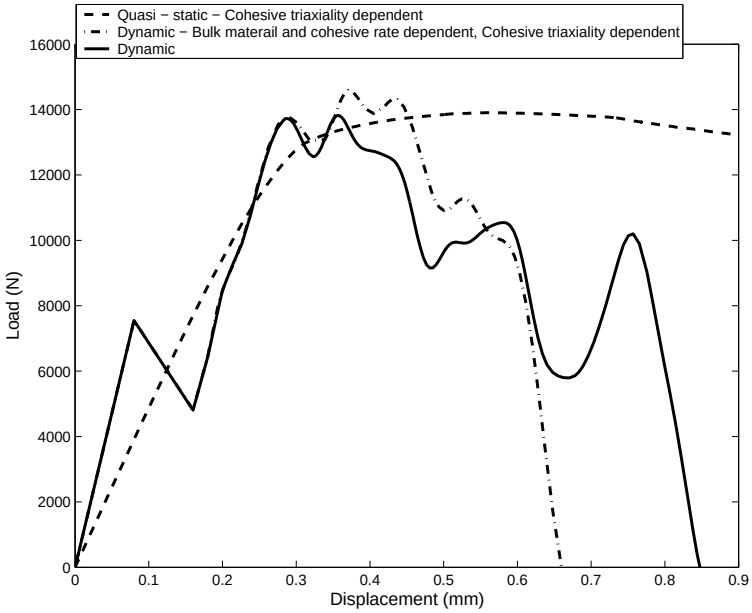

Figure 18: A general comparison between quasi static and dynamic cases

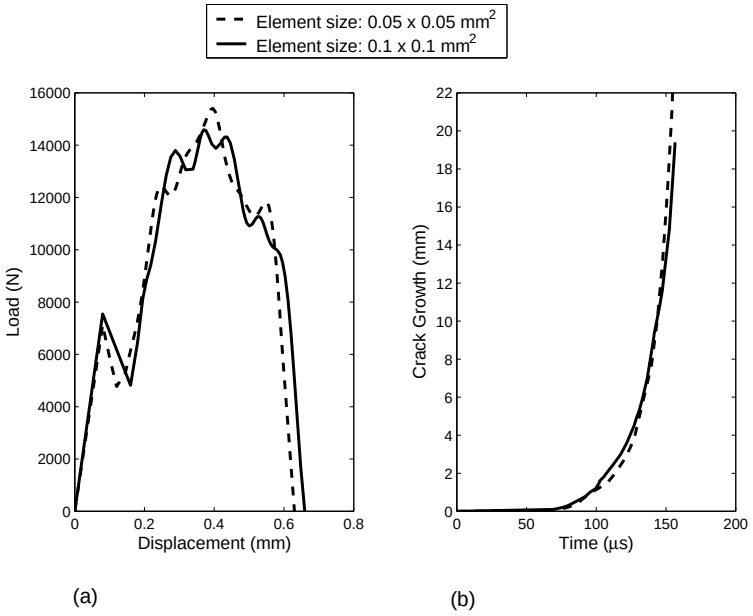

Figure 19: The effect of element size on (a) load-displacement curve, (b) crack growth